

DFT study of solvation of Li^+/Na^+ in fluoroethylene carbonate/vinylene carbonate/ethylene sulfite solvents for lithium/sodium-based battery

Qi Liu(刘琦), Guoqiang Tan(谭国强), Feng Wu(吴锋), Daobin Mu(穆道斌), and Borong Wu(吴伯荣)
Citation: Chin. Phys. B, 2021, 30 (**3**): 038203. DOI: 10.1088/1674-1056/abd763
Journal homepage: http://cpb.iphy.ac.cn; http://iopscience.iop.org/cpb

What follows is a list of articles you may be interested in

Comparative calculation on Li^+ solvation in common organic electrolyte solvents for lithium ion batteries

Qi Liu(刘琦), Feng Wu(吴锋), Daobin Mu(穆道斌), Borong Wu(吴伯荣)
Chin. Phys. B, 2020, 29 (**4**): 048202. DOI: 10.1088/1674-1056/ab75cc

Performance of n-type silicon/silver composite anode material in lithium ion batteries: A study on effect of work function matching degree

Guo-Jun Xu(徐国军), Chen-Xin Jin(金晨鑫), Kai-Jie Kong(孔凯捷), Xi-Xi Yang(杨西西), Zhi-Hao Yue(岳之浩), Xiao-Min Li(李晓敏), Fu-Gen Sun(孙福根), Hai-Bin Huang(黄海宾), Lang Zhou(周浪)
Chin. Phys. B, 2018, 27 (**10**): 108201. DOI: 10.1088/1674-1056/27/10/108201

Gas treatment protection of metallic lithium anode

Wen-jun Li(李文俊), Quan Li(李泉), Jie Huang(黄杰), Jia-yue Peng(彭佳悦), Geng Chu(褚赓), Ya-xiang Lu(陆雅翔), Jie-yun Zheng(郑杰允), Hong Li(李泓)
Chin. Phys. B, 2017, 26 (**8**): 088202. DOI: 10.1088/1674-1056/26/8/088202

Conductivity and applications of Li-biphenyl-1, 2-dimethoxyethane solution for lithium ion batteries

Geng Chu(褚赓), Bo-Nan Liu(刘柏男), Fei Luo(罗飞), Wen-Jun Li(李文俊), Hao Lu(陆浩), Li-Quan Chen(陈立泉), Hong Li(李泓)
Chin. Phys. B, 2017, 26 (**7**): 078201. DOI: 10.1088/1674-1056/26/7/078201

Instability of lithium bis(fluorosulfonyl)imide (LiFSI)–potassium bis(fluorosulfonyl)imide (KFSI) system with $LiCoO_2$ at high voltage

Zhang Shu, Li Wen-Jun, Ling Shi-Gang, Li Hong, Zhou Zhi-Bin, Chen Li-Quan
Chin. Phys. B, 2015, 24 (**7**): 078201. DOI: 10.1088/1674-1056/24/7/078201

DFT study of solvation of Li^+/Na^+ in fluoroethylene carbonate/vinylene carbonate/ethylene sulfite solvents for lithium/sodium-based battery*

Qi Liu(刘琦)†, Guoqiang Tan(谭国强), Feng Wu(吴锋), Daobin Mu(穆道斌), and Borong Wu(吴伯荣)

Beijing Key Laboratory of Environment Science and Engineering, School of Material Science and Engineering, Beijing Institute of Technology, Beijing 100081, *China*

(Received 26 October 2020; revised manuscript received 8 December 2020; accepted manuscript online 30 December 2020)

Choosing suitable solvent is the key technology for the electrochemical performance of energy storage device. Among them, vinylene carbonate (VC), fluoroethylene carbonate (FEC), and ethylene sulfite (ES) are the potential organic electrolyte solvents for lithium/sodium battery. However, the quantitative relation and the specific mechanism of these solvents are currently unclear. In this work, density functional theory (DFT) method is employed to study the lithium/sodium ion solvation in solvents of VC, ES, and FEC. We first find that 4VC-Li^+, 4VC-Na^+, 4ES-Li^+, 4ES-Na^+, 4FEC-Li^+, and 4FEC-Na^+ are the maximum thermodynamic stable solvation complexes. Besides, it is indicated that the innermost solvation shells are consisted of 5VC-Li^+/Na^+, 5ES-Li^+/Na^+, and 5FEC-Li^+/Na^+. It is also indicated that the Li^+ solvation complexes are more stable than Na^+ complexes. Moreover, infrared and Raman spectrum analysis indicates that the stretching vibration of O = C peak evidently shifts to high frequency with the Li^+/Na^+ concentration reducing in *n*VC-Li^+/Na^+ and *n*FEC-Li^+/Na^+ solvation complexes, and the O = C vibration peak frequency in Na^+ solvation complexes is higher than that of Li^+ complexes. The S = O stretching vibration in *n*ES-Li^+/Na^+ solvation complexes moves to high frequency with the decrease of the Li^+/Na^+ concentration, the S = O vibration in *n*ES-Na^+ is higher than that in *n*ES-Li^+. The study is meaningful for the design of new-type Li/Na battery electrolytes.

Keywords: elelctrolyte, solvation, lithium ion battery, sodium ion battery

PACS: 82.20.Yn, 82.45.Gj, 82.47.Aa **DOI:** 10.1088/1674-1056/abd763

1. Introduction

Lithium ion battery has been applied in kinds of electric devices,[1–4] and sodium ion battery is very promising for large-scale grid energy storage system.[5–7] The electrochemical performance is closely related to the electrolyte property of lithium/sodium ion battery.[8–12] The functional solvents are necessary to optimize lithium/sodium battery electrochemical performance.[13–16]

Vinylene carbonate (VC), fluorinated ethylene carbonate (FEC), and ethylene sulfite (ES), etc. solvents were usually used as electrolyte additives to improve the lithium/sodium ion battery interface stability.[17–26] The research on their potential application as electrolyte solvents is also important. Wang *et al.* have investigated FEC organic solvent containing LiTFSI (0.75 mol·kg^{-1}) salt as electrolyte to improve the safety of graphite||NMC based lithium ion battery by reducing flammability.[27] The 1.2 M FEC based electrolyte with $LiPF_6$ salt has been used in Li/Li and Cu/$LiFePO_4$ cells, forming nanostructured LiF particles SEI film and improving the electrochemical performance.[28] Lee *et al.* have demonstrated that FEC-based electrolyte with 1 M NaFSI salt stabilizes Na metal deposition during electrochemical cycling, the FEC–NaFSI constructs the NaF, Na_2CO_3, and sodium alkylcarbonates mechanically strong and ion-permeable interlayer.[29] FEC based co-solvent of FEC + DMC has been proposed for Mg_2Si anode of lithium ion battery to improve cycling stability by forming LiF-rich SEI.[30] The FEC based FEC/TTE/DEC (2:2:1 vol.) mixed electrolyte has been used in anode-free battery of $LiNi_{0.5}Mn_{0.3}Co_{0.2}O_2$/Cu, forming LiF-richer SEI on the anode surface, improving the cycling performance of the battery.[31] FEC solvent in the $Li_4Ti_5O_{12}$/$LiNi_{0.5}Mn_{1.5}O_4$ battery for the anti-oxidation electrolyte system has improved the electrochemical performance, FEC solvent is responsible the formation of stable, uniform SEI films on individual $Li_4Ti_5O_{12}$ particles.[32] FEC based electrolyte with FEC/dimethyl carbonate/HFE mixed solvents has been used to improve the performance of both lithium metal anode and high voltage $LiCoO_2$ cathode material.[33] Zeng *et al.* have proposed a fluorinated intermixture of FEC and di-(2,2,2 trifluoroethyl) carbonate (TFEC) based non-flammable electrolyte for lithium/sodium ion battery, improving the compatibility with Prussian blue sodium ion battery cathode and the cycling stability of the silicon nanoparticle anode of lithium ion battery.[34,35] *In-situ* Na deposition image has indicated that

*Project supported by the International Science & Technology Cooperation of China (Grant No. 2016YFE0102200), the National Natural Science Foundation of China (Grant No. 51902024), the Fundamental Research Funds for the Central Universities, China, the National Postdoctoral Program for Innovative Talents of China (Grant No. BX20180038), China Postdoctoral Science Foundation (Grant No. 2019M650014), and Beijing Natural Science Foundation, China (Grant No. L182022).

†Corresponding author. E-mail: liuqi985@bit.edu.cn

© 2021 Chinese Physical Society and IOP Publishing Ltd

the use of ethylene carbonate (EC), DEC, and PC based electrolyte produces a large number of dendrites and gas releasing, and FEC co-solvent dramatically reduces the dendrite growth and gas releasing, meanwhile improves the cycling stability.[36] Kuratani *et al.* have studied the density, viscosity, and conductivity of 1.5–2.0 mol·dm^{-3} XClO$_4$ (X = Li and Na) based electrolyte in PC and γ-butyrolactone, the NaClO$_4$ based electrolyte enjoys higher ionic conductivity and lower viscosity compared with LiClO$_4$, and the ionic conductivity of NaClO$_4$ based electrolyte is 10%–20% higher than that of LiClO$_4$.[37] The density, viscosity, and ionic conductivity of Li- and Na-TFSI in γ-butyrolactone and PC based electrolytes at the condition of 0.1 mol/L $\leq C \leq$ 2.0 mol/L and 278 K $\leq T \leq$ 328 K have been investigated to understand the electrolyte solution chemistry, it is indicated that sodium ion electrolyte occupies more volume compared with lithium ion electrolyte, and sodium ion electrolyte enjoys higher mobility and conductivity.[38] Zhang *et al.* have reported vinylethylene carbonate (VEC) single solvent based electrolyte with 1 M lithium hexafluorophosphates salt, enabling high safety and long cycle life for Li-metal batteries, which is attributed to unique interphase property and easy Li$^+$ desolvation in VEC.[39] Jin *et al.* have found that the aliphatic chain and cross-linking poly(ethylene oxide) (PEO) with carboxylate and carbonate species SEIs are formed in pure VC or FEC electrolytes.[40] Sulfur-containing sulfolane based solvent has been developed, which enhances the Li$^+$ conductivity of NCA cathode SEI film and the interfacial stability.[41] Wu *et al.* have reported a novel ES based electrolyte for Li-O$_2$ batteries which shows excellent round-trip efficiency and high specific capacity.[42] Wang *et al.*'s study has indicated that the Li plating potential dropping is ascribed to the carbonate-containing unstable SEI layer,[43] and LiFSI improved lithium deposition in carbonate electrolyte.[44] Cosolvation of Li$^+$ and solvent reductive decomposition have been studied by density functional theory (DFT) method, indicating that the different interactions with Li$^+$ affect the formation of SEI film.[45] Quantum chemistry (QC) calculations have been used for the prediction of oxidation and reduction stability of electrolyte components such as EC, FEC, and VC.[13] Liu *et al.*'s study has indicated that the different solvation ionic numbers lead to the different HOMO levels.[9] DFT calculation also has been used to study the reduction mechanism of VC, ES, and FEC for lithium/sodium battery.[15,46] The oxidation/reduction potentials and decomposition of VC have been studied by quantum chemistry calculation.[47–49] The concerns of the researchers are mainly focused on the influence of electrolyte solvents to the SEI formation mechanism and the improvement of the electrochemical performance of the battery, the research on the solvation mechanism of Li$^+$/Na$^+$ in FEC, VC, ES, etc. organic solvents is absent. We have studied the Li$^+$/Na$^+$ solvation in commonly used carbonate esters and ethers based on previous studies.[50,51] It is important for understanding the performance improvement mechanism of lithium/sodium ion battery by comparing the Li$^+$/Na$^+$ solvation property in these organic solvents.

The Li$^+$/Na$^+$ solvation property in organic electrolyte solvents of VC, ES, and FEC is mainly investigated in this work. The energy, solvation structures, infrared spectrum, Raman spectrum, Gibbs free energy, and enthalpy of Li$^+$/Na$^+$-solvation complexes are compared. It is demonstrated that the solvation complexes of Li$^+$ with VC, ES, and FEC solvents are more stable compared with Na$^+$ solvation complexes. The discussion of detail method and result will be shown in the next part.

2. Computation method

B3LYP nonlocal correlation functional was used for the DFT calculations. The optimizations of structure and calculation of frequency were completed at B3LYP/6-311++G(d,p) level, the theoretical spectra analysis was obtained from frequency calculation. For more accurate calculation, B3LYP/6-311++G(3df,3dp) was used for all of the single point energy computation, and the energy was revised by zero-point energy calculation. ΔG = ΔThermal correction to Gibbs free energy (B3LYP/6-311+G(d,p)) + ΔE (B3LYP/6-311++G(3df,3dp)). ΔH = ΔThermal correction to enthalpy (B3LYP/6-311+G(d,p)) + ΔE (B3LYP/6-311++G(3df,3dp)). Enthalpies and Gibbs free energies were calculated at 298.15 K. Gaussian 09 program package was used for all DFT calculations.[52]

3. Results and discussion

3.1. Li$^+$/Na$^+$ solvation in VC solvent

The Gibbs free energy curves of stepwise Li$^+$ and Na$^+$ solvation reactions to VC solvent in different ions concentration are shown in Fig. 1(a). It is clearly exhibited that with VC molecule increasing, the ΔG for the stepwise reaction gradually increases, and when forming 4VC-Li$^+$ and 4VC-Na$^+$ solvation complexes, thermodynamic equilibrium for the reactions is reached. The ΔE, ΔH, and ΔG of the VC stepwise solvation reactions with Li$^+$ and Na$^+$ are exhibited in Table 1.

Table 1. The ΔE, ΔH, and ΔG of VC stepwise solvation reactions with Li$^+$ and Na$^+$, the unit is kcal·mol^{-1}.

Reactions	ΔE	ΔH	ΔG
VC + Li$^+$ = VC-Li$^+$	–46.10	–46.63	–39.54
VC + VC-Li$^+$ = 2VC-Li$^+$	–34.94	–34.37	–26.75
VC + 2VC-Li$^+$ = 3VC-Li$^+$	–21.48	–20.82	–13.64
VC + 3VC-Li$^+$ = 4VC-Li$^+$	–12.94	–12.26	–2.88
VC + 4VC-Li$^+$ = 5VC-Li$^+$	–3.57	–2.75	6.23
VC + Na$^+$ = VC-Na$^+$	–33.40	–33.65	–26.93
VC + VC-Na$^+$ = 2VC-Na$^+$	–26.96	–26.22	–19.4
VC + 2VC-Na$^+$ = 3VC-Na$^+$	–19.10	–18.31	–11.28
VC + 3VC-Na$^+$ = 4VC-Na$^+$	–13.45	–12.54	–5.95
VC + 4VC-Na$^+$ = 5VC-Na$^+$	–6.69	–5.88	2.73

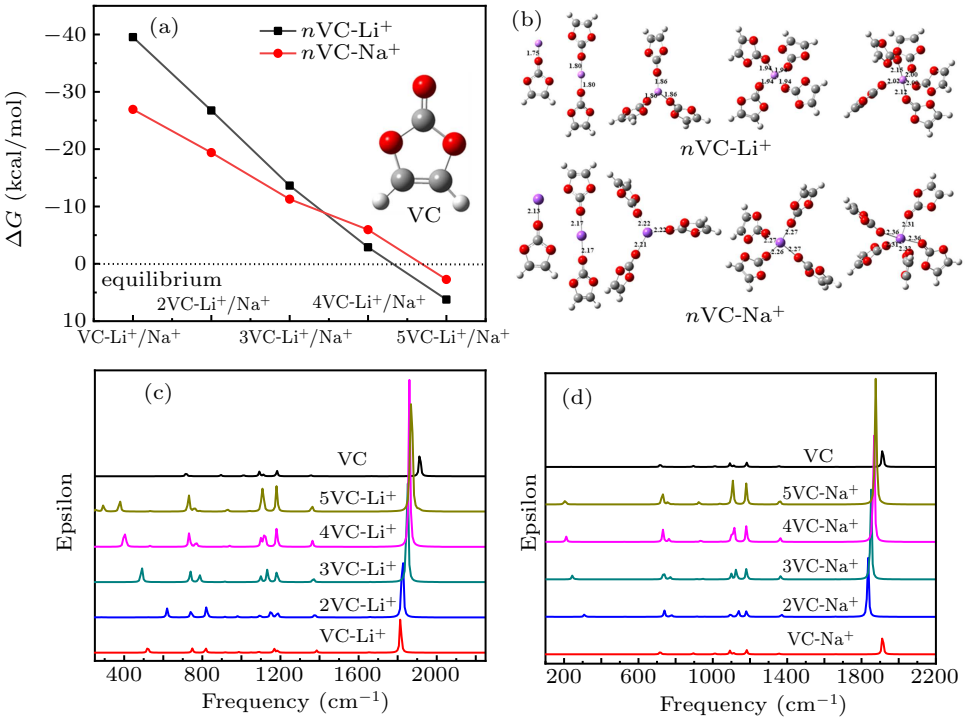


Fig. 1. (a) The Gibbs free energy curves of stepwise Li^+ and Na^+ solvation reactions to VC solvent in different ions concentration. (b) nVC-Li^+ and nVC-Na^+ ($1 \le n \le 5$) solvation complexes models. IR spectra of (c) nVC-Li^+ and (d) nVC-Na^+ complexes by DFT calculation.

It can be seen that the ΔG of stepwise solvation reactions VC + 4VC-Na^+ = 5VC-Na^+ and VC + 4VC-Li^+ = 5VC-Li^+ are 2.73 kcal·mol^{-1} and 6.23 kcal·mol^{-1}, respectively, indicating that stepwise reactions to form 5VC-Li^+ and 5VC-Na^+ solvation complexes are non-spontaneous processes.

Table 2. Lengths of all Li–O and Na–O bonds and the average length after optimization for nVC-Li^+ and nVC-Na^+ complexes, the units are Å.

VC-Li^+	1.75					1.75 (average)
2VC-Li^+	1.80	1.80				1.80 (average)
3VC-Li^+	1.86	1.86	1.86			1.86 (average)
4VC-Li^+	1.94	1.94	1.94	1.94		1.94 (average)
5VC-Li^+	2.15	2.00	2.00	2.12	2.02	2.06 (average)
VC-Na^+	2.13					2.13 (average)
2VC-Na^+	2.17	2.17				2.17 (average)
3VC-Na^+	2.22	2.22	2.21			2.22 (average)
4VC-Na^+	2.27	2.27	2.27	2.26		2.27 (average)
5VC-Na^+	2.36	2.31	2.36	2.31	2.32	2.33 (average)

The nVC-Li^+ and nVC-Na^+ ($1 \le n \le 5$) solvation complexes models are shown in Fig. 1(b), the solvation complexes are formed by VC molecules surrounding of Li^+/Na^+, and 5VC-Li^+ and 5VC-Na^+ complexes are still the innermost solvation shells. The interaction between Li^+/Na^+ and VC is carbonyl oxygen, which is in accord with the results that the first solvation shell is formed between Li^+ and the carbonyl oxygen atom of VC in Bolimowska *et al.*'s study.[53] In addition, the average Li–O bond lengths are 1.75 Å, 1.80 Å, 1.86 Å, 1.94 Å, and 2.06 Å in VC-Li^+, 2VC-Li^+, 3VC-Li^+, 4VC-Li^+, and 5VC-Li^+ solvation complexes, respectively, as shown in Table 2; and the average Na–O bond lengths are 2.13 Å, 2.17 Å, 2.22 Å, 2.27 Å, and 2.33 Å in VC-Na^+, 2VC-Na^+, 3VC-Na^+, 4VC-Na^+, and 5VC-Na^+, respectively. The solvation ionic radii of 3VC-Li^+, 4VC-Li^+, and 5VC-Li^+ are 6.101 Å, 6.231 Å, and 6.331 Å, respectively. The radii of 3VC-Na^+, 4VC-Na^+, and 5VC-Na^+ are 6.452 Å, 6.542 Å, and 6.638 Å, respectively. The solvation ionic radius increases with the VC molecules increase for the nVC-Li^+/Na^+ complexes, and the ionic radii of nVC-Na^+ are evidently larger than those of nVC-Li^+.

Figure 1(c) exhibits the theoretical IR spectra of nVC-Li^+. The vibration peak in 1815.01–1873.59 cm^{-1} frequency range represents the stretching vibration of O = C in nVC-Li^+ solvation complexes, and with the Li^+ concentration reducing in nVC-Li^+, the O = C peak evidently shifts to high frequency and the C = O bond is shortened (Table S1), it is in accord with the experimental FTIR spectrum results that O = C stretching vibration of VC is attributed to the peak at 1836 cm^{-1}.[54] Besides, the three peaks in 1362.82–1385.38 cm^{-1}, 1181.17–1185.41 cm^{-1}, and 1111.97–1168.08 cm^{-1} frequency ranges represent different O–C stretching and H–C twist vibrations, when the Li^+ concentration decreases, all the above three vibration peaks shift to low frequency, and the peak in 1111.97–1168.08 cm^{-1} exhibits the maximum frequency shift. The peak in 762.18–822.216 cm^{-1} frequency range represents Li–O stretching accompanying with carbonate stretching in nVC-Li^+ solvation complexes, when the concentration of lithium ion decreases from 2VC-Li^+ to 5VC-Li^+, the vibration peak moves to low frequency, while the peak shifts to high frequency from VC-Li^+ to 2VC-Li^+. The peak in 731.559–748.953 cm^{-1} represents C–H twisting vibration in different nVC-Li^+ solvation complexes, the vibration shifts to low fre-

quency with the decrease of Li^+ concentration. The Li–O stretching vibration in nVC-Li^+ solvation complexes is assigned to 376.039–619.7 cm^{-1} frequency range which moves to low frequency when the complex changes from 2VC-Li^+ to 5VC-Li^+. Figure 1(d) exhibits the theoretical IR spectra for nVC-Na^+. From the figure, the peak in 1828.89–1878.62 cm^{-1} represents the stretching vibration of O=C in nVC-Na^+ solvation complexes, with the sodium ion concentration decreasing, the vibration peak moves to high frequency and the C=O bond is shortened (Table S2). The frequency movement rule of nVC-Na^+ solvation complexes is in agreement with that of nVC-Li^+. The results show that the different interactions of Li^+ and Na^+ with VC lead to the different C=O bond vibration peaks for the two kinds of solvation complexes, and the C=O vibration peak frequency in the nVC-Na^+ solvation complexes is higher than that of nVC-Li^+, the difference becomes smaller when the solvent number increases in the complexes. Besides, the three peaks in 1360.26–1373.95 cm^{-1}, 1180.81–1182.38 cm^{-1}, and 1109.49–1148.71 cm^{-1} represent different stretching of O–C and H–C twisting in nVC-Na^+ solvation complexes, the vibration peak shifts to low frequency with the decrease of Na^+ concentration. The vibration frequencies of the above three peaks in nVC-Na^+ solvation complexes are lower than those in nVC-Li^+ complexes. The vibration peak in 759.056–782.01 cm^{-1} represents stretching of Na–O accompanying with carbonate stretching vibration, which moves to low frequency with the Na^+ concentration decreasing in the complexes. The vibration peak in 729.712–744.412 cm^{-1} represents the twisting of H–C in the solvation complexes of nVC-Na^+, the peak shifts to low frequency with the decrease of Na^+ concentration. The twisting vibration frequency of H–C in nVC-Na^+ complexes is slightly lower than that in nVC-Li^+. The stretching vibration of Na–O in nVC-Na^+ solvation complexes is assigned to 208.76–310.102 cm^{-1} frequency range, the vibration peak shifts to low frequency when the sodium ion concentration changes from 2VC-Na^+ to 5VC-Na^+.

On the other hand, the theoretical Raman spectra analysis of nVC-Li^+ complexes is exhibited in Fig. 2(a), the vibration peaks in 3294.66–3321.08 cm^{-1} represent stretching vibration of H–C in nVC-Li^+ solvation complexes. The C=C bond stretching vibration peak in nVC-Li^+ complexes is assigned to the frequency range of 1654.26–1661.37 cm^{-1}, which slightly moves to high frequency when the Li^+ concentration decreases in the solvation complexes. The two Raman vibration peaks in 1183.43–1185.41 cm^{-1} and 1089.18-1102.01 cm^{-1} represent stretching of O–C accompanying with twisting vibration of C–H. The three vibration peaks in 1046.16-1050.88 cm^{-1}, 941.29–986.518 cm^{-1}, and 911.503–918.111 cm^{-1} represent different stretching of O–C in nVC-Li^+ solvation complexes. The C–H twisting vibration peak in nVC-Li^+ solvation complexes is assigned to 847.531–857.607 cm^{-1}, which moves to low frequency when the Li^+ concentration decreases. Besides, the Raman vibration peak in 768.177–817.172 cm^{-1} represents Li–O stretching accompanying with carbonate stretching in nVC-Li^+ complexes, it is fundamentally in accord with the peak frequency of IR spectra. Figure 2(b) shows the theoretical Raman spectra of nVC-Na^+, the two peaks in 3293.52–3320.97 cm^{-1} and 1658.01–1662.73 cm^{-1} represent the stretching vibrations of C–H and C=C bonds respectively in the nVC-Na^+ solvation complexes. There is small difference for C–H and C=C vibration peak frequencies in nVC-Na^+ and nVC-Li^+ complexes, indicating that the interaction to C–H and C=C bonds is negligible between Li^+/Na^+ and VC. In addition, the C–O stretching vibration in nVC-Na^+ complexes is assigned to the two peaks of 1039.52–1049.47 cm^{-1} and 929.064–964.543 cm^{-1}, which move to low frequency with the sodium ion concentration decreasing. The Raman vibration peak in 843.097–854.053 cm^{-1} frequency range represents twisting of H–C in nVC-Na^+ complexes. The Raman vibration peak in 759.056–782.01 cm^{-1} represents stretching of Na–O accompanying with carbonate stretching in nVC-Na^+.

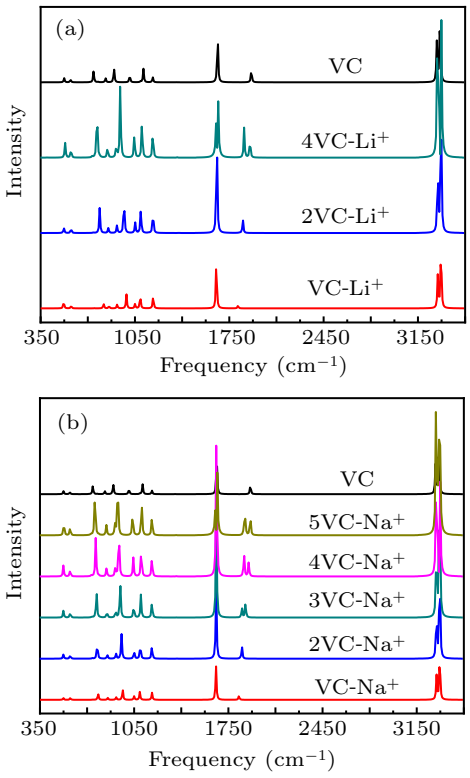


Fig. 2. Raman spectra of (a) nVC-Li^+ and (b) nVC-Na^+ by DFT calculation.

3.2. Li^+/Na^+ solvation in ES solvent

Except for VC solvent, the solvation of Li^+/Na^+ in ES solvent is also studied. The Gibbs free energy curves of stepwise Li^+ and Na^+ solvation reactions to ES solvent in different ions concentration are exhibited in Fig. 3(a). The thermodynamic equilibrium is reached after forming 4ES-Li^+ and

4ES-Na^+ for the stepwise solvation reactions. Table 3 exhibits ΔE, ΔH, and ΔG of the ES stepwise solvation reactions with Li^+ and Na^+. The ΔG for reactions ES + 4ES-Li^+ = 5ES-Li^+ and ES + 4ES-Na^+ = 5ES-Na^+ are 12.96 kcal·mol^{-1} and 3.49 kcal·mol^{-1}, respectively, suggesting non-spontaneous reaction processes to form 5ES-Li^+ and 5ES-Na^+ complexes.

Table 3. The ΔE, ΔH, and ΔG of ES stepwise solvation reactions with Li^+ and Na^+, the unit is kcal·mol^{-1}.

Reactions	ΔE	ΔH	ΔG
ES + Li^+ = ES-Li^+	–45.83	–46.36	–39.17
ES + ES-Li^+ = 2ES-Li^+	–34.55	–33.95	–25.85
ES + 2ES-Li^+ = 3ES-Li^+	–20.38	–19.78	–11.05
ES + 3ES-Li^+ = 4ES-Li^+	–13.39	–13.26	–3.25
ES + 4ES-Li^+ = 5ES-Li^+	–2.33	–1.83	12.96
ES + Na^+ = ES-Na^+	–32.68	–32.93	–26.13
ES + ES-Na^+ = 2ES-Na^+	–26.34	–25.59	–18.22
ES + 2ES-Na^+ = 3ES-Na^+	–18.37	–18.2	–7.17
ES + 3ES-Na^+ = 4ES-Na^+	–13.56	–14.37	–1.28
ES + 4ES-Na^+ = 5ES-Na^+	–6.29	–3.77	3.49

Figure 3(b) shows the nES-Li^+ and nES-Na^+ ($1 \leq n \leq 5$) solvation complexes models, the inner most solvation shell is consisted of five ES molecules surrounding Li^+/Na^+ to form 5ES-Li^+ and 5ES-Na^+ complexes at the S = O bond. As shown in Table 4, the average bond lengths of Li–O are 1.75 Å, 1.80 Å, 1.86 Å, 1.94 Å, and 2.07 Å, respectively, in ES-Li^+, 2ES-Li^+, 3ES-Li^+, 4ES-Li^+, and 5ES-Li^+; and the average bond lengths of Na–O are 2.12 Å, 2.16 Å, 2.21 Å, 2.26 Å, and 2.33 Å, respectively, in ES-Na^+, 2ES-Na^+, 3ES-Na^+, 4ES-Na^+, and 5ES-Na^+. The solvation ionic radii of 3ES-Li^+, 4ES-Li^+, and 5ES-Li^+ are 6.087 Å, 6.182 Å, and 6.323 Å, respectively. The radii of 3ES-Na^+, 4ES-Na^+, and 5ES-Na^+ are 6.412 Å, 6.507 Å, and 6.586 Å, respectively. The results demonstrate that the average O–Na and O–Li bonds are stretched with the solvent number increasing in the complexes, and the ionic radius of the solvation complex is enlarged. On the other hand, the ionic radius of Na^+ solvation complexes in ES is larger than that of Li^+ solvation complexes.

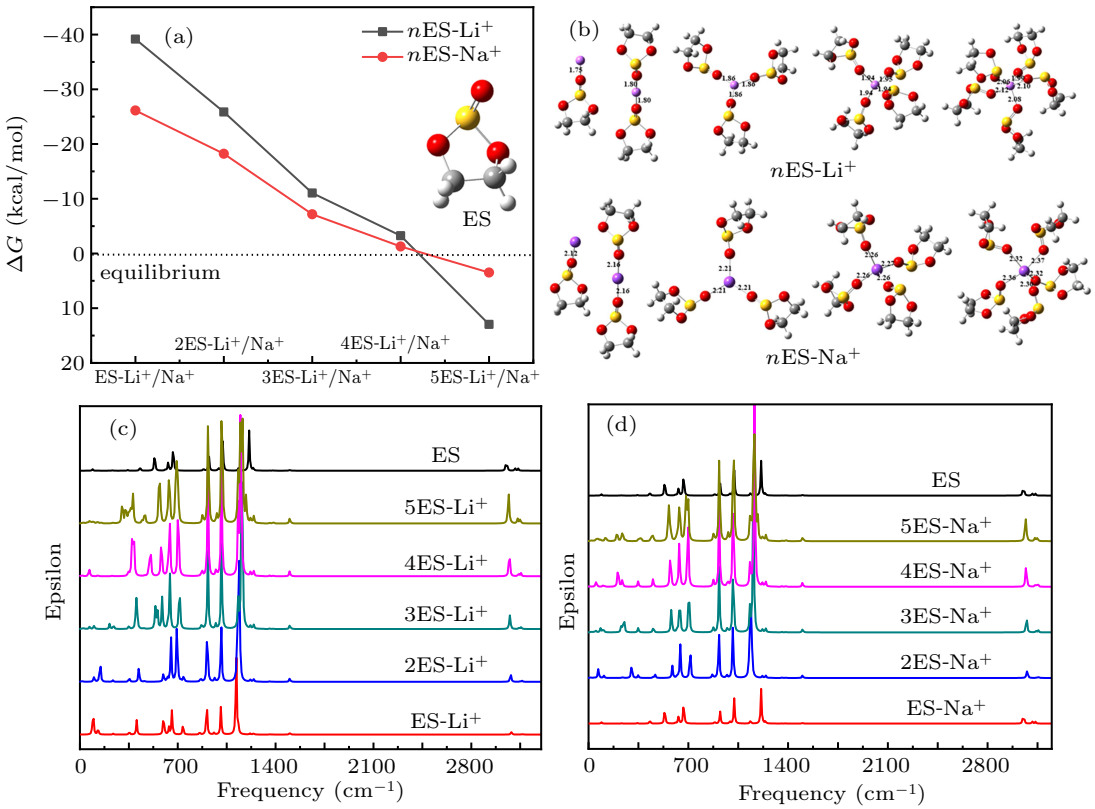


Fig. 3. (a) The Gibbs free energy curves of stepwise Li^+ and Na^+ solvation reactions to ES solvent in different ions concentration. (b) nES-Li^+ and nES-Na^+ ($1 \leq n \leq 5$) solvation complexes models. IR spectra of (c) nES-Li^+ and (d) nES-Na^+ complexes by DFT calculation.

In addition, IR spectra of nES-Li^+ complexes by DFT calculation are shown in Fig. 3(c), the S = O stretching vibration in nES-Li^+ solvation complexes is assigned to 1118.3–1189.37 cm^{-1} frequency range, which moves to high frequency with the decrease of Li^+ concentration, and the S = O bond is also shortened (Table S3). The two peaks in 1008.79–1020.66 cm^{-1} and 907.372-922.035 cm^{-1} represent different stretching vibrations of O–C–C–O bonds, which move to high frequency with Li^+ concentration decreasing. Besides, the O–S–O symmetrical stretching vibration in nES-Li^+ solvation complexes is assigned to 692.627–742.714 cm^{-1}, which moves to low frequency from 2ES-Li^+ to 5ES-Li^+. The peak in the frequency range of 640.685–658.844 cm^{-1} represents the asymmetric vibration of O–S–O in nES-Li^+ solvation complexes, the peak moves to low frequency with Li^+ concentration decreasing in the complexes. The peak in 565.743–

598.221 cm^{-1} represents the asymmetric vibration of O–S–O; and it shifts to low frequency from 2ES-Li$^+$ to 5ES-Li$^+$. The peak in the frequency range of 303.443–421.853 cm^{-1} represents O–Li stretching driving sulfite stretching, and the vibration peak shifts to low frequency from 2ES-Li$^+$ to 5ES-Li$^+$.

Table 4. Length of all Li-O and Na–O bonds and the average length after optimization for *n*ES-Li$^+$ and *n*ES-Na$^+$ complexes, the units are Å.

ES-Li$^+$	1.75					1.75 (average)
2ES-Li$^+$	1.80	1.80				1.80 (average)
3ES-Li$^+$	1.86	1.86	1.86			1.86 (average)
4ES-Li$^+$	1.94	1.95	1.94	1.94		1.94 (average)
5ES-Li$^+$	2.06	1.99	2.1	2.08	2.12	2.07 (average)
ES-Na$^+$	2.12					2.12 (average)
2ES-Na$^+$	2.16	2.16				2.16 (average)
3ES-Na$^+$	2.21	2.21	2.21			2.21 (average)
4ES-Na$^+$	2.26	2.27	2.26	2.26		2.26 (average)
5ES-Na$^+$	2.36	2.32	2.37	2.32	2.30	2.33 (average)

On the other hand, the IR spectra of *n*ES-Na$^+$ complexes by DFT calculation are exhibited in Fig. 3(d), the peak in the frequency range of 1126.8–1165.37 cm^{-1} represents the stretching vibration of S = O in the *n*ES-Na$^+$. The two peaks in 1012.19–1016.07 cm^{-1} and 912.811-917.813 cm^{-1} are on behalf of different stretching vibrations of O–C–C–O. Besides, the symmetric stretching vibration of O–S–O group in *n*ES-Na$^+$ complexes is assigned to the frequency of 681.309–719.991 cm^{-1}, which moves to low frequency with Na$^+$ concentration decreasing; because of the different interaction of ES molecules to Li$^+$/Na$^+$, the symmetric stretching vibration peak frequency in the *n*ES-Na$^+$ complexes is evidently lower than that in *n*ES-Li$^+$ complexes. The two peaks in 638.527–647.396 cm^{-1} and 558.312–593.845 cm^{-1} represent asymmetrical O–S–O stretching vibration in the *n*ES-Na$^+$ complexes. Furthermore, the stretching vibration of Na–O in the *n*ES-Na$^+$ complexes is assigned to the frequency of 200.708–302.905 cm^{-1}.

Figure 4(a) shows the Raman spectra of *n*ES-Li$^+$ by DFT calculation. The C–H stretching vibration in *n*ES-Li$^+$ complexes is assigned to the peak in the frequency range of 3070.12–3167.78 cm^{-1}. Besides, the three peaks at about 1500 cm^{-1}, 1242 cm^{-1}, and 1218 cm^{-1} represent different C–H twisting vibrations in *n*ES-Li$^+$ complexes. The S = O Raman stretching vibration frequency in the *n*ES-Li$^+$ complexes is assigned to 1118.3–1178.31 cm^{-1}. The two Raman peaks in 1008.79–1012.39 cm^{-1} and 907.372–919.306 cm^{-1} represent different stretching vibrations of O–C–C–O in the *n*ES-Li$^+$ complexes. The Raman vibration peak in 708.235–737.643 cm^{-1} represents symmetrical O–S–O stretching vibration in the *n*ES-Li$^+$ complexes.

On the other hand, the Raman spectra of *n*ES-Na$^+$ by DFT calculation are shown in Fig. 4(b), the Raman stretching vibration of C–H in the *n*ES-Na$^+$ solvation complexes is assigned to the peak of 3063.18–3162.13 cm^{-1}. The three Raman peaks in 1500.38–1503.32 cm^{-1}, 1242.33–1243.68 cm^{-1}, and 1218.87–1221.83 cm^{-1} represent the different twisting vibrations of C–H in the *n*ES-Na$^+$ solvation complexes, the vibration peak frequency of C–H twisting in *n*ES-Na$^+$ complexes is slightly higher than that in *n*ES-Li$^+$. The S = O Raman stretching vibration in *n*ES-Na$^+$ is assigned to the frequency of 1126.8–1186.42 cm^{-1}, and the S = O vibration frequency in *n*ES-Na$^+$ complexes is higher than that in *n*ES-Li$^+$. In addition, the two Raman peaks in 1012.19–1016.07 cm^{-1} and 912.811–919.593 cm^{-1} represent different stretching vibrations of O–C–C–O in *n*ES-Na$^+$ complexes. The symmetric O–S–O Raman stretching vibration in *n*ES-Na$^+$ is assigned to the peak of 689.831–719.991 cm^{-1}.

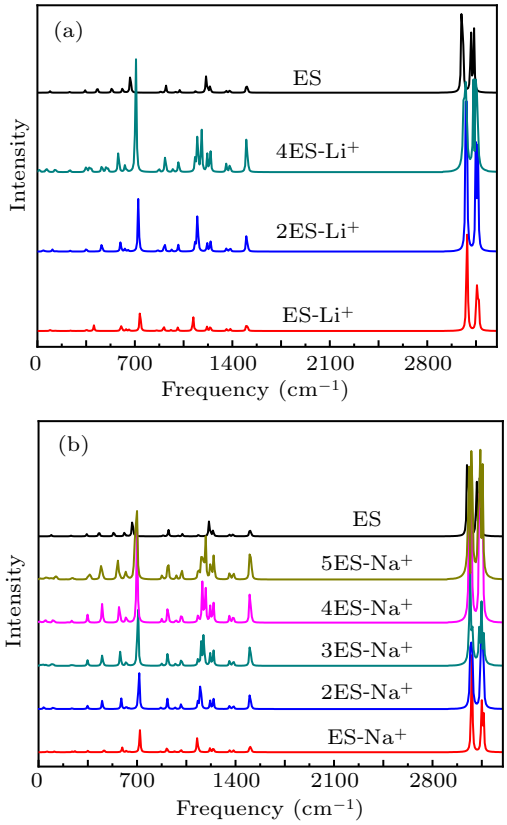


Fig. 4. Raman spectra of (a) *n*ES-Li$^+$ and (b) *n*ES-Na$^+$by DFT calculation.

3.3. Li$^+$/Na$^+$ solvation in FEC solvent

The Gibbs free energy curves of stepwise Li$^+$ and Na$^+$ solvation reactions to FEC solvent in different ions concentration are shown in Fig. 5(a). The thermodynamic equilibrium is reached when forming 4FEC-Li$^+$ and 4FEC-Na$^+$ by stepwise solvation reaction. The ΔE, ΔH, and ΔG of the FEC stepwise solvation reactions with Li$^+$ and Na$^+$ are exhibited in Table 5. The reactions FEC + 4FEC-Li$^+$ = 5FEC-Li$^+$ and FEC + 4FEC-Na$^+$ = 5FEC-Na$^+$ are non-spontaneous processes. Figure 5(b) shows the *n*FEC-Li$^+$ and *n*FEC-Na$^+$ ($1 \leq n \leq 5$) solvation complexes models, it is exhibited that Na$^+$/Li$^+$ combine FEC forming the innermost solvation shells of 5FEC-Li$^+$ and 5FEC-Na$^+$. The average Li–O and Na–

O bonds are stretched in the Li^+/Na^+-solvation complexes with the FEC molecules increasing (see Table 6). The solvation ionic radii of 3FEC-Li^+, 4FEC-Li^+, and 5FEC-Li^+ are 5.995 Å, 6.138 Å, and 6.393 Å, respectively. The radii of 3FEC-Na^+, 4FEC-Na^+, and 5FEC-Na^+ are 6.319 Å, 6.429 Å, and 6.508 Å, respectively. It means that the solvation ionic radius is enlarged; and the ionic radii of the *n*FEC-Na^+ solvation complexes are larger than those of *n*FEC-Li^+. Figure 5(c) exhibits the IR spectra of *n*FEC-Li^+ complexes by DFT calculation, the C = O stretching vibration peak in *n*FEC-Li^+ complexes is assigned to the frequency of 1806.48–1885.42 cm^{-1} which moves to high frequency when the Li^+ concentration decreases, and the C = O bond in *n*FEC-Li^+ is shortened (Table S5). The two peaks in 1237.59-1249.21 cm^{-1} and 1173.4–1220.35 cm^{-1} represent stretching of carbonate C–O accompanying with twisting vibration of C–H in *n*FEC-Li^+ complexes, and the two peaks shift to low frequency with the concentration of Li^+ decreases in the complex. The two peaks in the frequency ranges of 1124.87–1147.62 cm^{-1} and 1090.17–1107 cm^{-1} represent stretching of O–C accompanying with stretching vibration of C–F in *n*FEC-Li^+ complexes, and the above two peaks shift to low frequency with the decrease of the Li^+ concentration. The CH_2–O stretching driving C–F stretching vibration peak in the *n*FEC-Li^+ complexes is assigned to the frequency of 1003.95–1014.95 cm^{-1}. In addition, the peak in 744.505–796.389 cm^{-1} represents O–Li stretching and carbonate stretching vibration in the *n*FEC-Li^+ complexes. The peak in 273.604–622.67 cm^{-1} represents O-Li stretching vibration in the *n*FEC-Li^+ complexes, the peak moves to low frequency from 2FEC-Li^+ to 5FEC-Li^+.

Table 5. The ΔE, ΔH, and ΔG of FEC stepwise solvation reactions with Li^+ and Na^+, the unit is kcal·mol^{-1}.

Reactions	ΔE	ΔH	ΔG
FEC + Li^+ = FEC-Li^+	–45.48	–45.95	–39
FEC + FEC-Li^+ = 2FEC-Li^+	–34.38	–33.79	–25.81
FEC + 2FEC-Li^+ = 3FEC-Li^+	–21.45	–20.76	–13.41
FEC + 3FEC-Li^+ = 4FEC-Li^+	–12.98	–12.27	–3.72
FEC + 4FEC-Li^+ = 5FEC-Li^+	–3.31	–2.47	8.44
FEC + Na^+ = FEC-Na^+	–32.92	–33.13	–26.51
FEC + FEC-Na^+ = 2FEC-Na^+	–26.48	–25.74	–18.28
FEC + 2FEC-Na^+ = 3FEC-Na^+	–18.95	–18.12	–11.61
FEC + 3FEC-Na^+ = 4FEC-Na^+	–13.43	–13.1	–3.68
FEC + 4FEC-Na^+ = 5FEC-Na^+	–7.96	–6.86	5.08

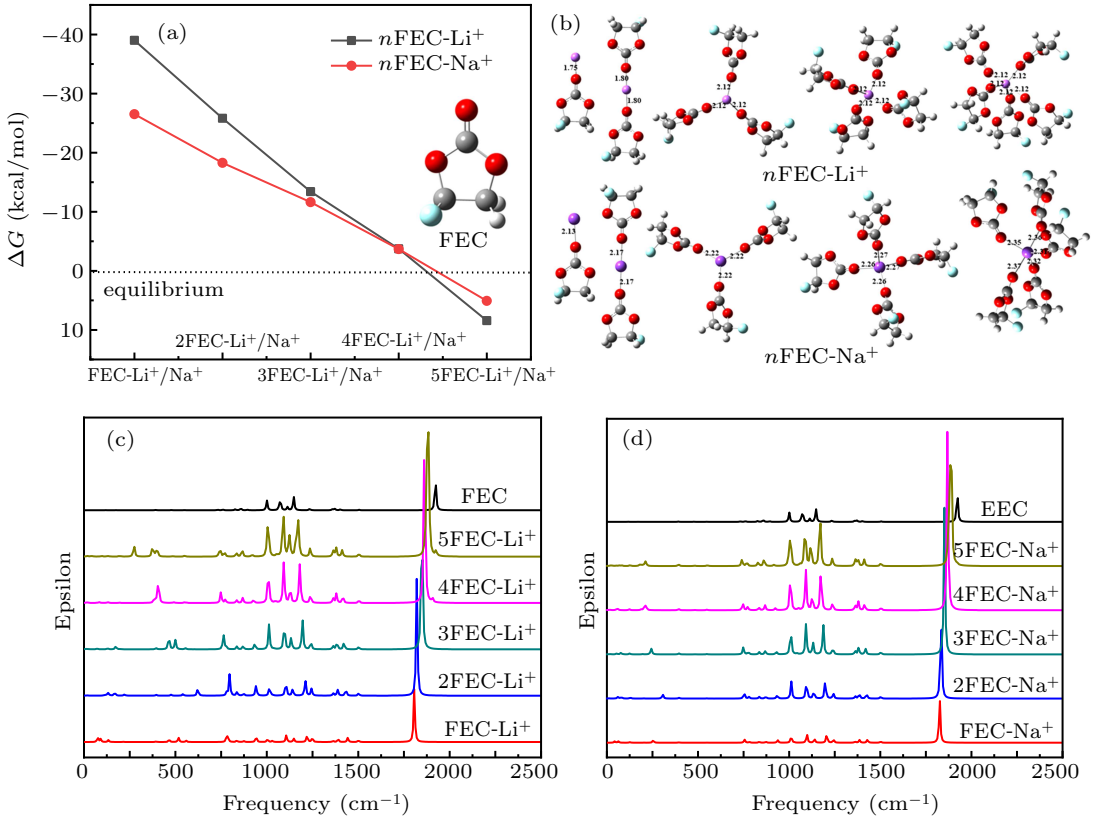


Fig. 5. (a) The Gibbs free energy curves of stepwise Li^+ and Na^+ solvation reactions to FEC solvent in different ions concentration. (b) *n*FEC-Li^+ and *n*FEC-Na^+ ($1 \leq n \leq 5$) solvation complexes models. IR spectra of (c) *n*FEC-Li^+ and (d) *n*FEC-Na^+ complexes by DFT calculation.

On the other hand, the IR spectra of *n*FEC-Na^+ complexes by DFT calculation are exhibited in Fig. 5(d), the C = O stretching vibration peak in the *n*FEC-Na^+ complexes is assigned to the frequency of 1825.67–1889.31 cm^{-1}, with the concentration of Na^+ decreasing the peak shifts to high frequency and the C = O bond is shortened (Table S6). The frequency of C = O stretching vibration peak for *n*FEC-Na^+ complexes is higher than that of *n*FEC-Li^+. The two peaks in 1238.07–1243.58 cm^{-1} and 1168.54–1206.39 cm^{-1} represent stretching of O–C accompanying with twisting of C–H

vibration in *n*FEC-Na^+, and the vibration frequency moves to low frequency with the sodium ion concentration decreasing. Besides, the two peaks in 1119.07–1138.99 cm^{-1} and 1088.06–1097.41 cm^{-1} represent stretching of C–O accompanying with stretching of C–F, and the peaks also shift to low frequency with the sodium ion concentration decreasing in the *n*FEC-Na^+ complexes. The CH_2–O stretching driving C–F stretching vibration in the *n*FEC-Na^+ is assigned to the peak in the frequency range of 1007.36–1011.62 cm^{-1}. Furthermore, the peak in 741.512–755.315 cm^{-1} represents O–Na stretching accompanying with carbonate stretching vibration in the *n*FEC-Na^+ complexes, which moves to low frequency with the sodium ion concentration decreasing in the complexes. The O–Na stretching vibration peak in the *n*FEC-Na^+ is assigned to the frequency of 211.156–306.307 cm^{-1}.

Table 6. Lengths of all Li-O and Na–O bonds and the average length after optimization for *n*FEC-Li^+ and *n*FEC-Na^+ complexes, the units are Å.

FEC-Li^+	1.75					1.75 (average)
2FEC-Li^+	1.80	1.80				1.80 (average)
3FEC-Li^+	1.86	1.86	1.86			1.86 (average)
4FEC-Li^+	1.94	1.94	1.94	1.94		1.94 (average)
5FEC-Li^+	1.98	2.32	1.99	1.98	2.06	2.07 (average)
FEC-Na^+	2.13					2.13 (average)
2FEC-Na^+	2.17	2.17				2.17 (average)
3FEC-Na^+	2.22	2.22	2.22			2.22 (average)
4FEC-Na^+	2.27	2.27	2.26	2.26		2.27 (average)
5FEC-Na^+	2.31	2.37	2.32	2.35	2.36	2.34 (average)

Figure 6(a) shows the Raman spectra of *n*FEC-Li^+ by DFT calculation. The C–H stretching vibration in the *n*FEC-Li^+ solvation complexes is assigned to the frequency of 3099.54–3319.78 cm^{-1}. The peak at about 1501 cm^{-1} represents twisting vibration of C–H in the *n*FEC-Li^+ complexes. The FEC ring enlargement vibration in the *n*FEC-Li^+ complexes is assigned to the frequency of 926.229–941.81 cm^{-1} which moves to low frequency with the lithium ion concentration decreasing. The Raman peak in 867.656–873.965 cm^{-1} represents stretching vibration of C–C in *n*FEC-Li^+ complexes, and the peak shifts to low frequency with the decrease of the Li^+ concentration. Besides, the Raman peak in 748.187–779.833 cm^{-1} represents O-Li stretching accompanying with carbonate stretching vibration in the *n*FEC-Li^+ complexes.

On the other hand, figure 6(b) exhibits the Raman spectra of *n*FEC-Na^+ by DFT calculation. The C–H stretching vibration peak in the *n*FEC-Na^+ complexes is assigned to the frequency of 3085.76–3170.68 cm^{-1}, which moves to low frequency with sodium ion concentration decreasing. The Raman peak at about 1503 cm^{-1} represents twisting vibration of C–H in the *n*FEC-Na^+ complexes. The FEC ring enlargement stretching vibration peak in the *n*FEC-Na^+ complexes is assigned to the frequency of 916.897–937.212 cm^{-1}. The peak in 860.869–872.501 cm^{-1} is ascribed to stretching vibration of C–C in the *n*FEC-Na^+ complexes, and the peak moves to low frequency with the sodium ion concentration decreasing. Besides, the peak in 742.024–755.315 cm^{-1} represents stretching of Na–O accompanying with stretching vibration of carbonate, the vibration peak moves to low frequency with the sodium ion concentration decreasing.

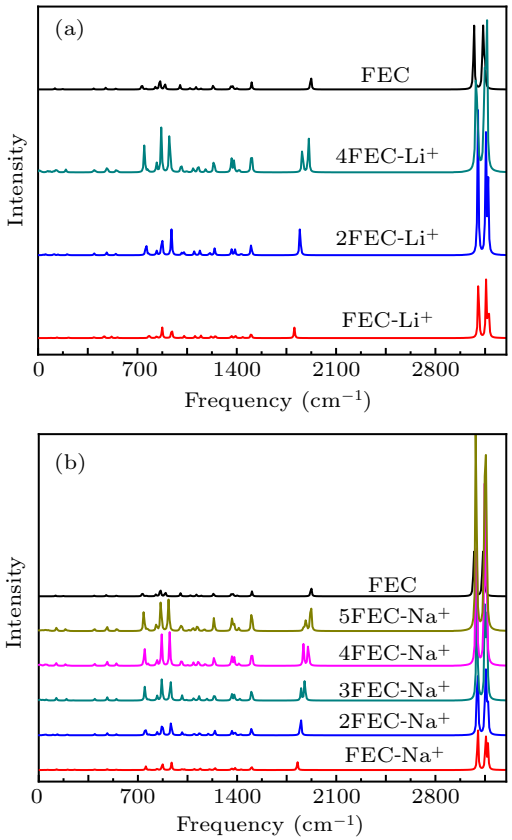


Fig. 6. Raman spectra of (a) *n*FEC-Li^+ and (b) *n*FEC-Na^+ by DFT calculation.

At last, the stepwise solvation reactions and total solvation reactions Gibbs free energy change ΔG for Li^+/Na^+ in the potential electrolyte solvents of VC, ES, and FEC are analyzed. Figure 7(a) shows the Gibbs free energy curve for Li^+/Na^+ stepwise solvation reactions in VC, ES, and FEC, respectively, with solvent numbers changed. The maximum thermodynamics stability solvation complexes are consisted of 4VC-Li^+, 4VC-Na^+, 4ES-Li^+, 4ES-Na^+, 4FEC-Li^+, and 4FEC-Na^+ by spontaneous solvation reactions between Li^+/Na^+ and VC, ES, FEC solvents. Figure 7(b) shows the Gibbs free energy curve for the overall Li^+/Na^+ solvation reactions with the change of solvation numbers. It is clearly seen that the absolute value of Gibbs free energy releasing (ΔG) reaches the maximum by overall Li^+/Na^+ solvation reactions forming 4sol-Li^+/Na^+ complexes, which is in agreement with the above stepwise solvation reaction results. In addition, it is clearly exhibited that the absolute values of free energy releasing (ΔG) for forming lithium-ion solvation complexes of *n*VC-Li^+, *n*ES-Li^+, *n*FEC-Li^+ are evidently larger than those for formation of *n*VC-Na^+, *n*ES-Na^+, *n*FEC-Na^+

complexes, indicating that lithium ion is easier to combine with VC, ES, and FEC compared to sodium ion, and lithium-ion solvation complexes of *n*VC-Li^+, *n*ES-Li^+, and *n*FEC-Li^+ are more stable compared with *n*VC-Na^+, *n*ES-Na^+, and *n*FEC-Na^+ sodium ion solvation complexes.

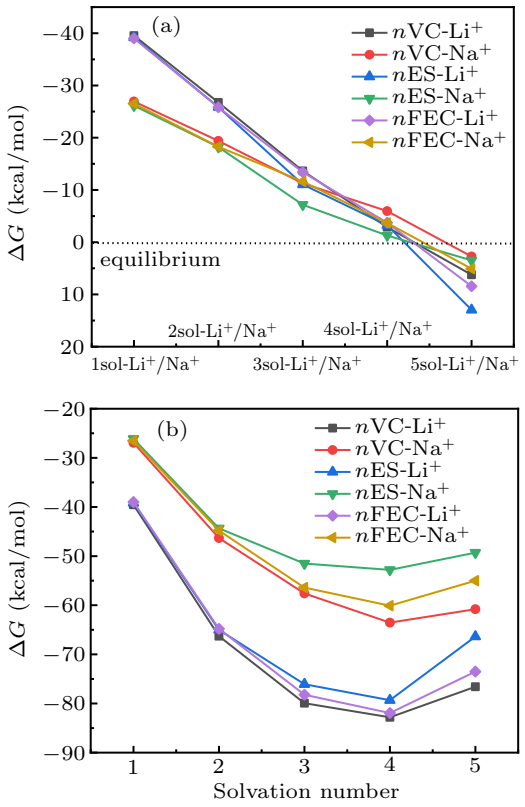


Fig. 7. (a) Gibbs free energy curves for Li^+/Na^+ stepwise solvation reactions in VC, ES, and FEC, respectively, with solvent numbers changed. (b) Gibbs free energy curve for the overall Li^+/Na^+ solvation reactions with the change of solvation numbers.

4. Conclusion

Electrolyte solvents are very important to the electrochemical performance of lithium/sodium batteries. The solvation property of lithium/sodium ion in organic electrolyte solvents of VC, ES, and FEC is studied by DFT method. The results demonstrate that the maximum thermodynamics stability solvation complexes are consisted of 4VC-Li^+, 4VC-Na^+, 4ES-Li^+, 4ES-Na^+, 4FEC-Li^+, and 4FEC-Na^+. The innermost solvation shells of 5VC-Li^+, 5VC-Na^+, 5ES-Li^+, 5ES-Na^+, 5FEC-Li^+, and 5FEC-Na^+ can be formed between Li^+/Na^+ and solvent molecules. In addition, the results demonstrate that lithium ion is easier to combine with VC, ES, and FEC compared to sodium ion, and lithium-ion solvation complexes of *n*VC-Li^+, *n*ES-Li^+, and *n*FEC-Li^+ are more stable than *n*VC-Na^+, *n*ES-Na^+, and *n*FEC-Na^+ sodium ion solvation complexes. Besides, the theoretical IR and Raman spectra analysis for the solvation complexes between Li^+/Na^+ and VC, ES, FEC solvents demonstrates that the stretching vibration of O = C peak evidently shifts to high frequency when Li^+/Na^+ concentration reducing in *n*VC-Li^+, *n*VC-Na^+, *n*FEC-Li^+, and *n*FEC-Na^+ solvation complexes, and the O = C vibration in the Na^+ solvation complexes is higher than that of Li^+ complexes. The S = O vibration frequency in *n*ES-Na^+ complexes is higher than that of *n*ES-Li^+, and the S = O stretching vibration in *n*ES-Li^+/Na^+ solvation complexes moves to high frequency with the decrease of Li^+/Na^+ concentration. Besides, the stretching vibration of O–S–O group in *n*ES-Na^+/Li^+ complexes moves to low frequency with ion concentration decreasing, and the peak in *n*ES-Na^+ complexes is lower than that of *n*ES-Li^+. The vibration peaks frequency occurs regular shift when the Li^+/Na^+ concentration changes, and the different interactions for Li^+ and Na^+ with these solvents lead to the diverse characteristic peak frequencies for Li^+/Na^+ solvation complexes. The results are important to guide the design of electrolyte and understand the performance improvement mechanism of lithium/sodium battery. In addition, different solvation complexes concentration may affect the reduction/oxidation potential, and solvation ionic is important for the initial stages of SEI formation. More studies on oxidation/reduction potentials of different solvation ionics are needed to deeply analyze the formation mechanism of the SEI film.

References

[1] Goodenough J B and Park K 2013 *J. Am. Chem. Soc.* **135** 1167
[2] Schmuch R, Wagner R, Horpel G, Placke T and Winter M 2018 *Nat. Energy* **3** 267
[3] Huang L X, Chen Y F, Li P J, Huan R, He J R, Wang Z G, Hao X, Liu J B, Zhang W L and Li Y R 2012 *Acta Phys. Sin.* **61** 156103 (in Chinese)
[4] Bai Y, Wang B and Zhang W F 2011 *Acta Phys. Sin.* **60** 068202 (in Chinese)
[5] Yang Z, Zhang J, Kintnermeyer M C, Lu X, Choi D, Lemmon J P and Liu J 2011 *Chem. Rev.* **111** 3577
[6] Yabuuchi N, Kubota K, Dahbi M and Komaba S 2014 *Chem. Rev.* **114** 11636
[7] Hwang J Y, Myung S and Sun Y 2017 *Chem. Soc. Rev.* **46** 3529
[8] Xu K 2014 *Chem. Rev.* **114** 11503
[9] Liu Q, Xu H, Wu F, Mu D, Shi L, Wang L, Bi J and Wu B 2019 *ACS Appl. Energy Mater.* **2** 8878
[10] Ponrouch A, Monti D, Boschin A, Steen B, Johansson P and Palacin M R 2015 *J. Mater. Chem.* **3** 22
[11] Wang Y and Balbuena P B 2005 *Int. J. Quantum Chem.* **102** 724
[12] Zhang S, Li W J, Ling S G, Li H, Zhou Z B and Chen L Q 2015 *Chin. Phys. B* **24** 078201
[13] Delpa S A, Borodina O, Olguina M, Eisnerb C G, Allena J L T and Jow R 2016 *Electrochim. Acta* **209** 498
[14] Zhang Y, Krishnamurthy D and Viswanathan V 2020 *J. Electrochem. Soc.* **167** 070554
[15] Liu Q, Mu D, Wu B, Wang L, Gai L and Wu F 2017 *ChemSusChem* **10** 786
[16] Shigenobu K, Dokko K, Watanabe M and Ueno K 2020 *Phys. Chem. Chem. Phys.* **22** 15214
[17] Qian Y, Niehoff P, Borner M, Grutzke M, Monnighoff X, Behrends P, Nowak S, Winter M and Schappacher F M 2016 *J. Power Sources* **329** 31
[18] Heine J, Hilbig P, Qi X, Niehoff P, Winter M and Bieker P 2015 *J. Electrochem. Soc.* **162** A1094
[19] Jaumann T, Balach J, Langklotz U, Sauchuk V, Fritsch M, Michaelis A, Teltevskij V, Mikhailova D, Oswald S, Klose M, Stephani G, Hauser R, Eckert J and Giebeler L 2017 *Energy Storage Mater.* **6** 26

[20] Zhang B, Metzger M, Solchenbach S, Payne M, Meini S, Gasteiger H A, Garsuch A and Lucht B L 2015 *J. Phys. Chem. C* **119** 11337

[21] Zhu Z, Tang Y, Lv Z, Wei J, Zhang Y, Wang R, Zhang W, Xia H, Ge M and Chen X 2018 *Angew. Chem. Int. Edit.* **57** 3656

[22] Komaba S, Ishikawa T, Yabuuchi N, Murata W, Ito A and Ohsawa Y 2011 *ACS Appl. Mater. Inter.* **3** 4165

[23] Ji L, Gu M, Shao Y, Li X, Engelhard M H, Arey B W, Wang W, Nie Z, Xiao J, Wang C, Zhang J G and Liu J 2014 *Adv. Mater.* **26** 2901

[24] Takenaka N, Sakai H, Suzuki Y, Uppula P and Nagaoka M 2015 *J. Phys. Chem. C* **119** 18046

[25] Lee Y, Lee J, Kim H, Kang K and Choi N 2016 *J. Power Sources* **320** 49

[26] Liu Q, Yang G, Liu S, Han M, Wang Z and Chen L 2019 *ACS Appl. Mater. Interfaces* **11** 17435

[27] Wang Z, Hofmann A and Hanemann T 2019 *Electrochim. Acta* **298** 960

[28] Brown Z L, Jurng S, Nguyen C C and Lucht B L 2018 *ACS Appl. Energy Mater.* **1** 3057

[29] Lee Y, Lee J, Lee J, Kim K, Cha A, Kang S, Wi T, Kang S J, Lee H and Choi N 2018 *ACS Appl. Mater. Interfaces* **10** 15270

[30] Men F, Zhong H, Song Z and Zhan H 2018 *Mater. Chem. Phys.* **212** 131

[31] Jote B A, Beyene T T, Sahalie N A, Weret M A, Olbassa B W, Wondimkun Z T, Berhe G B, Huang C, Su W and Hwang B J 2020 *J. Power Sources* **461** 228102

[32] Liu J, Zhou L, Yu W and Yu A 2020 *J. Alloy Compd.* **812** 152064

[33] Lin S and Zhao J 2020 *ACS Appl. Mater. Interfaces* **12** 8316

[34] Zeng G, Liu Y, Gu C, Zhang K, An Y, Wei C, Feng J and Ni J 2020 *Acta Phys. -Chim. Sin.* **36** 1905006

[35] Zeng G, An Y, Xiong S and Feng J 2019 *ACS Appl. Mater. Interfaces* **11** 23229

[36] Rodriguez R, Loeffler K E, Nathan S S, Sheavly J K, Dolocan A, Heller A and Mullins C B 2017 *ACS Energy Lett.* **2** 2051

[37] Kuratani K, Uemura N, Senoh H, Takeshita H T and Kiyobayashi T 2013 *J. Power Sources* **223** 175

[38] Kuratani K, Kishimoto I, Nishida Y, Kondo R, Takeshita H T, Senoh H and Kiyobayashi T 2016 *J. Electrochem. Soc*. **163** H417

[39] Zhang Q, Liu S, Lin Z, Wang K, Chen M, Xu K and Li W 2020 *Nano Energy* **74** 104860

[40] Jin Y, Kneusels N H, Marbella L E, Castillo-Martínez E, Magusin P C M M, Weatherup R S, Jonsson E, Liu T, Paul S and Grey C P 2018 *J. Am. Chem. Soc.* **140** 9854

[41] Zhang F, Wang C, Zhao D, Yang L, Wang P, Li W, Wang B and Li S 2020 *Electrochim. Acta* **337** 135727

[42] Wu C, Liao C, Li L and Yang J 2016 *Chinese Chem. Lett.* **27** 1485

[43] Zhang S, Yang G, Liu S, Li X, Wang X, Wang Z and Chen L 2020 *Nano Energy* **70** 104486

[44] Yang G, Li Y, Liu S, Zhang S, Wang Z and Chen L 2019 *Energy Storage Mater.* **23** 350

[45] Wang Y and Balbuena P B 2005 *Int. J. Quant. Chem.* **102** 724

[46] Liu Q, Mu D, Wu B, Xu H, Wang L, Gai L, Shi L and Wu F 2017 *J. Electrochem. Soc*. **164** A3144

[47] Kang S, Park M H, Lee H and Han Y 2012 *Electrochem. Commun.* **23** 83

[48] Borodin O, Behl W and Jow T R 2013 *J. Phys. Chem. C* **117** 8661

[49] Zhang X, Pugh J K and Ross P N 2001 *J. Electrochem. Soc*. **148** E183

[50] Liu Q, Wu F, Mu D and Wu B 2020 *Phys. Chem. Chem. Phys.* **22** 2164

[51] Liu Q, Wu F, Mu D and Wu B. 2020 *Chin. Phys. B* **29** 048202

[52] Frisch M J, Trucks G W, Schlegel H B, Scuseria G E, Robb M A, Cheeseman J R, Scalmani G, Barone V, Mennucci B, Petersson G A *et al.* 2010 Gaussian 09, Gaussian, Inc., Wallingford, CT

[53] Bolimowska E, Castiglione F, Devemy J, Rouault H, Mele A, Padua A A H and Santini C C 2018 *J. Phys. Chem. B* **122** 8560

[54] Hongyou K, Hattori T, Nagai Y, Tanaka T, Nii H and Shoda K 2013 *J. Power Sources* **243** 72